Estimation and Analysis of Surface Heat Flux During Quenching in CNT Nanofluids

K. Babu
Department of Mechanical Engineering,
SSN College of Engineering,
Kalvakkam, Chennai 603110, India
e-mail: babuk@ssn.edu.in

T. S. Prasanna Kumar
Department of Metallurgical and Materials Engineering,
Indian Institute of Technology Madras,
Chennai 600036, India
e-mail: tsp@iitm.ac.in

In this article, water based carbon nanotube (CNT) nanofluids have been used as quenchants to study their effects on the heat transfer rate during immersion quenching. For this purpose, water based CNT nanofluids were prepared by dispersing CNTs with and without the use of surfactant. Quench probes with a diameter of 20 mm and a length of 50 mm were prepared from 304L stainless steel. Thermocouples were fixed at the selected location inside the quench probes and the probes were quenched in distilled water and CNT nanofluids. During quenching, time-temperature data were recorded using a data acquisition system. The heat flux and temperature at the quenched surface were estimated through the inverse heat conduction method. The computation results showed that the peak heat flux was higher by 37.5% during quenching in CNT nanofluid prepared without surfactant than that in water. However, surfactant assisted CNT nanofluid promoted a prolonged vapor phase during quenching and hindered the heat transfer rates significantly. The peak heat flux was dropped by 24.9% during quenching in CNT nanofluid prepared with surfactant as compared with its base fluid of water.
[DOI: 10.1115/1.4003572]

Keywords: CNT nanofluid, inverse heat conduction, surface heat flux, quenching

1 Introduction

Quenching is one of the important industrial processes in which the rate of heat transfer plays a vital role in the development of microstructure and mechanical properties of the quenched product. Heat transfer during quenching is complex and controlled by different cooling mechanisms. The parameters that affect the heat transfer during quenching may include surface temperature, surface roughness, agitation, thermophysical properties of the quenchant, and materials being quenched. The literature concerned with these various quenching parameters can be found in plenty. The heat transfer at the quenched surface is characterized by the surface heat flux or heat transfer coefficient of the quenching medium. The surface heat flux during quenching is unknown and calculated with the help of measured temperature data through inverse heat conduction (IHC) method.

Babu and Prasanna Kumar [1] estimated the surface heat flux and temperature using the IHC method for different initial soaking temperatures and modeled the surface heat flux as a function of dimensionless parameters during immersion quenching. Various algorithms for solving IHC problems have been well-documented by Beck et al. [2] and successfully implemented by many researchers [1–6]. Prasanna Kumar [3] described a serial solution method for a 2D IHC problem to estimate the heat flux in multiple segments and used it to estimate the heat flux components at the metal/mold interface in gravity die casting [4]. The same algorithm was used by Arunkumar et al. [5] to study the spatial variation of heat flux at the metal-mold interface. Sarmiento et al. [6] compared the results of the two computer programs developed for the estimation of heat transfer coefficient during quenching.

Intensive quenching (IQ) [7,8], known as IntensiQuench^{SM}, is an alternate way of hardening steel parts developed by Kobasko. IntensiQuench^{SM} process can be defined as cooling usually at a rate several times higher than the rate of normal or conventional quenching. Kobasko's research showed that very fast and very uniform part cooling actually reduced the probability of part cracking and distortion, while improving the surface hardness and durability of steel parts. In this perception, we wanted to achieve higher cooling rate during quenching possibly by the use of nanofluids. Nanofluids are the new class of engineering fluids and have attracted many researchers because of their better heat transfer performance [9–23]. Nanoparticles are suspended in the base fluids usually at a very low concentration to improve their heat transfer performance.

Choi [9] projected the possibility of using nanofluids for different practical applications including quenching. Narayan Prabhu and Fernades [10] used water and water based alumina nanofluid as quenchant and reported that the peak heat transfer coefficient of the nanoquenchant was 10% lower as compared with water. Kim et al. [11] conducted quenching experiments in pure water and water based nanofluids and showed that the quenching behavior of nanofluids was nearly identical with that of pure water. Lotfi and Shafii [12] investigated the boiling heat transfer characteristics of nanofluids by quenching a silver sphere in water based nanofluid and reported a considerable reduction in the quenching ability of nanofluids. These results on the use of nanofluids for quenching were not encouraging. However, Chopkar et al. [13,14] reported the higher quenching efficiency of water and ethylene glycol based nanofluids. The experiments conducted in Refs. [13,14] could not be treated as a practical quenching application since they quenched from 300°C to demonstrate the cooling performance of nanofluids.

Choi [9] stated that carbon nanotube (CNT) nanofluids yielded the highest heat transfer enhancement. Park and Jung [15] showed that the presence of CNTs improved the nucleate boiling heat transfer coefficient of water and R22, a refrigerant. Ding et al. [16] reported that nanofluids containing 0.5 wt % CNTs produced a maximum heat transfer enhancement of 350% by considering the flow conditions through a horizontal tube. Xie et al. [17] showed that the enhancement in thermal conductivities of CNT nanofluids was proportional to the CNT concentration. The different mechanisms for the improved heat transfer performance of

Contributed by the Heat Transfer Division of ASME for publication in the JOURNAL OF HEAT TRANSFER. Manuscript received February 22, 2010; final manuscript received February 1, 2011; published online April 1, 2011. Assoc. Editor: Patrick E. Phelan.

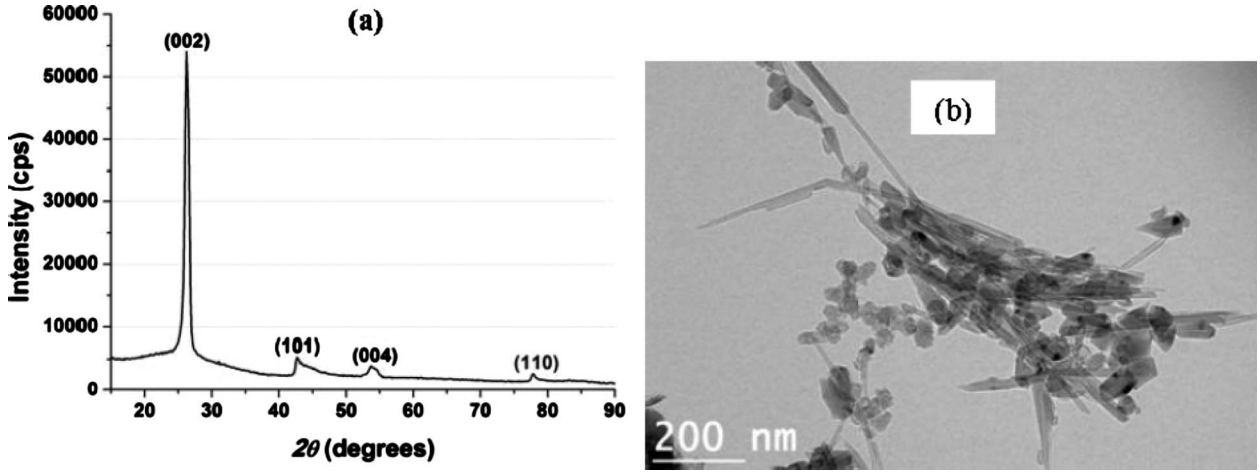

Fig. 1 (*a*) **XRD pattern of CNT and** (*b*) **TEM picture of CNT powder**

nanofluids were elaborated by Keblinski et al. [18]. The use of nanofluids for a practical quenching application reporting the improved heat transfer is not available until date.

The objective of this work is to use CNT nanofluids as quenchants to improve the heat transfer rate during quenching of steel parts. Multiwalled CNTs were synthesized through arc discharge method and dispersed in de-ionized (DI) water with and without surfactant for quenching application. Instrumented quench probes made of stainless steel (SS) 304L were quenched in water and CNT nanofluids and time-temperature data were recorded. The temperature data were used as input for the IHC algorithm to compute the unknown heat flux and temperature at the quenched surface. The results of the computation showed that CNT nanofluid prepared without surfactant resulted in a higher cooling rate than its base fluid, water. But, CNT nanofluids prepared with surfactant hindered the heat transfer rates significantly during quenching.

2 Preparation of CNT Nanofluids

Nanofluids refer to the fluids with suspended nanoparticles. By suspending nanoparticles at very low concentrations, usually 2 vol % or less in heating or cooling fluids, the heat transfer performance was proved to be significantly improved by the researchers. The basic idea is to increase the effective thermal conductivity of the base fluids to achieve better heat transfer performance. In the literature of nanofluids, the primary reason for the improved heat transfer performance of nanofluids is attributed to the higher effective thermal conductivity of nanofluids. Among different nanofluids, CNT nanofluids were reported to have higher heat transfer performance [9] because of their higher thermal conductivity, which is in the order of ~3000 W/m K (multiwalled CNT), and very high aspect ratio [16].

2.1 Synthesis and Characterization of CNT. Multiwalled CNTs were synthesized using an arc discharge method with a dc power supply, as described by Joshi et al. [24]. The detailed description of CNT synthesis for quenching application has been given by us in Ref. [25]. The synthesized CNT powder was characterized in X-ray diffractometer (Bruker D8 Discover, Madison, WI) with Cu $K\alpha$ radiation. The X-ray diffraction (XRD) pattern of the CNT powder is shown in Fig. 1(*a*). It has a peak at 26.29 deg, which corresponds with the (002) plane and confirms the highly graphitic structure of the CNT powder. The crystallite size was calculated to be 11.4 nm from the XRD pattern using Scherrer's formula. A pinch of CNT powder was then dispersed in 10 ml of de-ionized water through ultrasonication. A drop of this nanofluid was characterized using a transmission electron microscope (Philips CM12). The high resolution transmission electron microscopy (TEM) picture of CNT dispersion is shown in Fig. 1(*b*) in which CNT bundles are entangled and embedded in graphite spherulites. The minimum outer diameter of multiwalled CNTs observed was 9.73 nm and the average diameter ranged from 9 nm to 15 nm with a length ranging from few hundreds of nanometers to microns.

2.2 Preparation of CNT Nanofluid. The synthesized CNT powders were directly added to DI water to prepare the nanofluids at the required concentration. CNTs are known to be entangled and have a hydrophobic surface, which makes them to aggregate and settle down over time when dispersed in water. To disperse CNTs successfully in water, either surfactant should be used as in Refs. [16,20–22] or CNT should be functionalized by chemical treatments as in Refs. [17,18,23,26] to keep them suspended. Both the methods were equally followed in literature. The surfactants have their own bubble formation characteristics as they reduce the surface tension of the liquids. Because of this reason, it was expected that the presence of surfactants in nanofluids would alter the film boiling regime during quenching and influence the heat transfer rates significantly. So, CNT nanofluids were prepared by both the methods and used as quenchants.

A part of the CNT powders was functionalized by chemical treatment, as described in Refs. [18,26]. The acid treatment of CNTs involved soaking them in an acid mixture containing concentrated HNO_3 and H_2SO_4 in the ratio of 1:3 by volume for 5 h at room temperature. The chemical reaction in acid mixture forms a number of oxygen containing functional groups onto the CNT surface and turns them into hydrophilic to enable to prepare stable and homogeneous CNT nanofluids. The functionalized CNTs were termed as treated CNT (TCNT) and as produced CNTs were termed as pristine CNT (PCNT). Three samples of CNT nanofluids were prepared with and without the use of surfactant, Triton X100 [27], as per the following proportion:

(i) 30 ml of DI water+0.5 wt % of PCNT
(ii) 30 ml of DI water+0.5 wt % of TCNT
(iii) 30 ml of DI water+0.5 wt % of PCNT+2 wt % of Triton X100

The samples were sonicated at 20 kHz for 5 min in a probe type sonicator (Roop Telsonic, Mumbai, India). The nanofluid samples were studied for its stability by visual observation. The settlement of the nanofluid samples after 1 day and 1 week is shown in Figs. 2(*a*) and 2(*b*), respectively. Nanofluid sample (ii) exhibited a better stability over sample (i), and sample (iii) prepared with Triton X100 was stable for even months together.

For the quenching application, 2 l of nanofluid was prepared with 0.5 wt % of TCNTs without any surfactant. Thus, in 2 l of

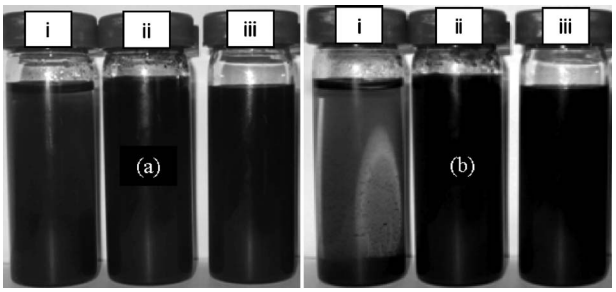

Fig. 2 (*a*) Nanofluid settling after 1 day and (*b*) nanofluid settling after 1 week

DI water, 10 g of TCNTs was added and dispersed by sonication for 1 h at 20 kHz. Another 2 l of nanofluid was prepared with 0.5 wt % of PCNTs and Triton X100 as a surfactant. 10 g of PCNTs was taken in a glass beaker and 15 g of Triton X100 surfactant was added and mixed well with a glass rod to wet the PCNTs completely. 2 l of DI water was added to this mixture and sonicated for 1 h at 20 kHz to obtain the well dispersed CNT nanofluid.

2.3 Characterization of CNT Nanofluid. Viscosity and wettability are the two basic fluid properties, which influence the heat transfer rates in fluids significantly. The contact angle of distilled water and CNT nanofluids on a SS substrate was measured using a goniometer (GBX, DGD-DX model, France) at room temperature of 27°C. The measured contact angle of water (case (i)), 0.5 wt % TCNT nanofluid (case (ii)), and 0.5 wt % PCNT nanofluid with the surfactant (case (iii)) on a SS substrate are shown in Fig. 3. The contact angle of case (ii) is lower than that of case (i), which is due to the presence of TCNTs in water. The contact angle of case (iii) is very much lower than that of case (i) or (ii) due to the presence of surfactant. Therefore, case (iii) can wet the surface of SS 304L much faster than case (i) or (ii).

Similarly, the dynamic viscosity of distilled water and CNT nanofluids was measured using a low viscosity rotational type viscometer (Brookfield DV-II+Pro, Middlebro, MA) at ~25°C and at a constant shear rate of 85.61 s^{-1}. A combination of cylindrical sample container and spindle called as Ultra Low Adapter (ULA), which can measure as low as 0.85 mPa s at 60 rpm, was used for taking measurements at low viscosity. The viscous drag experienced by the spindle in ULA was factory calibrated to display the dynamic viscosity on a digital output screen. First, the viscosity of distilled water was measured with different spindle speeds ranging from 100 rpm down to 60 rpm in a step of 10 rpm. It was found that at 25°C and at a spindle speed of 70 rpm (or at a shear rate of 85.61 s^{-1}), the viscosity of distilled water was 1.01 mPa s. Thus, the spindle speed was fixed at 70 rpm for measuring the viscosity of CNT nanofluids. The measured dynamic viscosity of water and CNT nanofluids prepared with and without the surfactant is plotted in Fig. 4.

3 Experimental Method

The design of cylindrical quench probes should consider the aspect (length to diameter) ratio. A commonly accepted design is to have an aspect ratio of 4–5, and a cylinder having this aspect ratio is called as "infinite cylinder." Under this condition, the heat

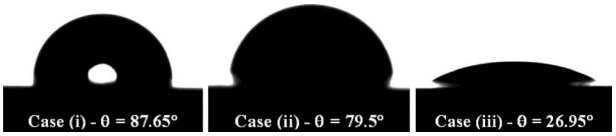

Fig. 3 Wettability of different quenchants used

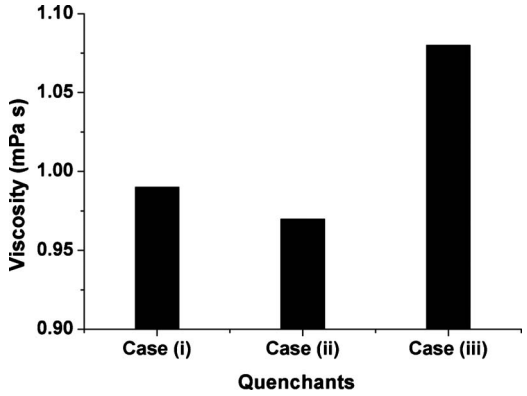

Fig. 4 Viscosity of different quenchants used

transfer would dominate in the radial direction and justify one dimensional heat transfer in the cylindrical probes. This is the common condition used in most of the laboratory cooling curve analysis during immersion quenching of cylindrical parts. Cylindrical quench probes with a diameter of 20 mm and a length of 50 mm (aspect ratio of 2.5) were used in this work. The probe design does not satisfy the condition of infinite cylinder. But, Chen et al. [28] used 1D and 2D finite element (FE) models for a quench probe having an aspect ratio of 2 and proved that the use of 1D and 2D FE models had a negligible difference. Moreover, the difficulties involved with the drilling of deep holes in SS posed a restriction on the probe length. Quench probes were prepared from SS 304L, which has no phase transformations during quenching. The schematic of the quench probes is given in Fig. 5(*a*) and the photograph of a quench probe fixed with the thermocouples is shown in Fig. 5(*b*).

Since the IHC analysis is very sensitive to the input temperature data, even small fluctuations in the input temperature data that result from measurement errors would be amplified in the results.

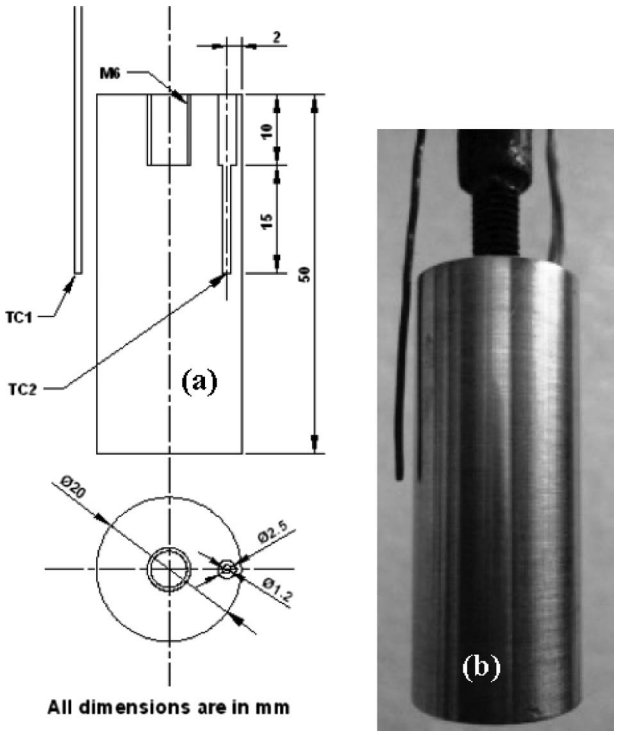

Fig. 5 (*a*) Schematic of the quench probes and (*b*) photograph of the quench probe showing the thermocouples

Therefore, care was taken during machining, selection, and mounting of thermocouples in the quench probes. The details of machining of the quench probes have been explained in Refs. [1,25]. Two mineral insulated K-type thermocouples with a wire diameter of 1 mm were used for temperature measurements during quenching. One of the thermocouples was calibrated at different temperatures ranging from 50°C to 600°C, and the maximum deviation between the equivalent millivolt and the actual millivolt produced was 0.34%. COREFIX (commercial adhesive paste) was used for fixing thermocouple TC2 after placing it carefully in its position and applying pressure until the paste was set. Another thermocouple (TC1) was tied along with the connecting stem such that its tip was at the midplane but ~2 mm away from the probe surface. Thermocouple TC1 was positioned diametrically opposite to TC2 so that its presence would not have any influence on the heat transfer near TC2 during quenching.

A fresh quench probe was used for each experiment. A vertical tubular electrical resistance furnace was used for heating the quenching probe. Once the probe was heated to 850°C, it was soaked for 30 min. The probe was released from its hook and, with the probe axis vertical, quickly immersed into a beaker containing 2 l of the quenchant. During quenching, neither the quenchant nor the probe was stirred. The quenchants used were distilled water, CNT nanofluids containing TCNT without surfactant, and PCNT with the surfactant. For convenience, the quenching in water is termed as case (i), in nanofluid containing TCNT is termed as case (ii), and in nanofluid containing PCNT with surfactant is termed as case (iii) throughout the remaining of this article. The quenchant temperature was maintained at ~30°C for all the experiments. The temperature recording for every 0.1 s was started using a computer assisted data acquisition system (Agilent—model 34970A, Loveland, CO) when the probe was in the furnace and continued until the probe temperature reached about 50°C during quenching.

4 Inverse Determination of Heat Flux and Surface Temperature

The unknown heat flux transients at the quenched surface were estimated using the IHC method from the measured temperature at TC2 during quenching. The serial IHC algorithm developed by Prasanna Kumar [3] was used in this work to estimate the heat flux transients at the probe-quenchant interface. The complete mathematical model and its implementation details of the serial IHC algorithm had been discussed elsewhere [3] and briefly summarized in Refs. [1,25] with respect to a quenching problem.

4.1 FE Model. A single unknown heat flux boundary was assumed along the probe-quenchant interface. Since the quench probes were immersed in the quenchant during quenching at a faster rate, the interface heat flux along the probe surface was not expected to vary much. The midsection of the quench probe, where the thermocouple tip was positioned, was taken as the model domain and neglected the end effects. Due to the circular geometry of quench probes, only a quadrant was taken as the model domain and discretized using a mesh of 1089 elements (three node triangular), and the total number of nodes was 595. The FE mesh showing the different boundary conditions is presented in Fig. 6. The thermophysical properties of SS 304L as a function of temperature taken from Ref. [1] were assigned to the FE model. The material properties were treated as stepwise linear within the given temperature range and were taken as constant outside the given temperature range. The effect of grid size and time step during inverse estimation of surface heat flux was reported by us in Ref. [1]. The suggested grid size of 1089 elements and a time step of 0.1 s were used in this work. The accuracy and reliability of the IHC method employed in this work to estimate the unknown heat flux at the quenched surface have already been proved in Ref. [1].

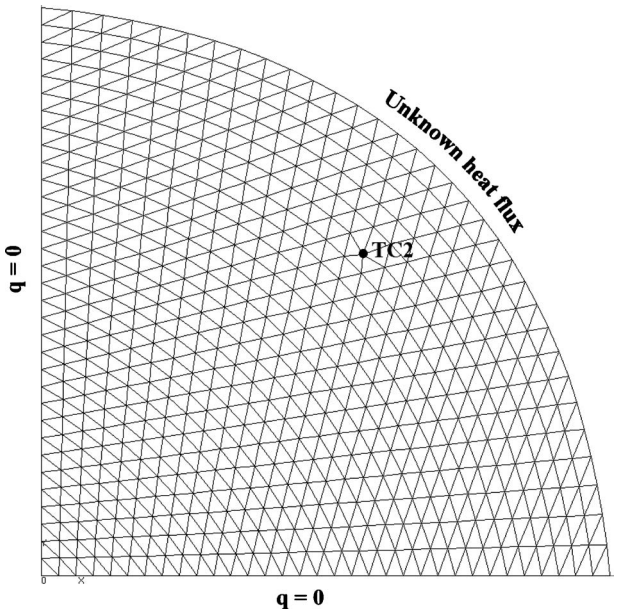

Fig. 6 FE mesh showing the TC2 location for the inverse estimation of surface heat flux

5 Results and Discussion

5.1 Experimental Data. The temperatures recorded by TC1 and TC2 during case (i), case (ii), and case (iii) quenching are shown in Fig. 7. The initial flattened portion corresponds with the temperatures recorded while the probes were in the furnace. The instant of probe's removal from the furnace is marked with "a" where TC1 and TC2 start deviating. The instant of full immersion is marked with "b" and was accurately located with the help of TC1 data as it drops instantaneously down to the quenchant temperature. Upon full immersion, the film boiling or vapor blanket stage takes place and the end of this stage is marked with "c" where the slope changes. This is the start of transition boiling and is followed by the nucleate boiling stage. The portion b to c of the cooling curves is the length of film boiling and it is longer in case (iii) followed by case (ii) and then by case (i).

When the temperature reaches ~100°C, there is a sudden drop in the cooling curves, which represents the start of convective cooling during quenching. The exact instant of the start of these different cooling stages would not be accurate if the calculation is

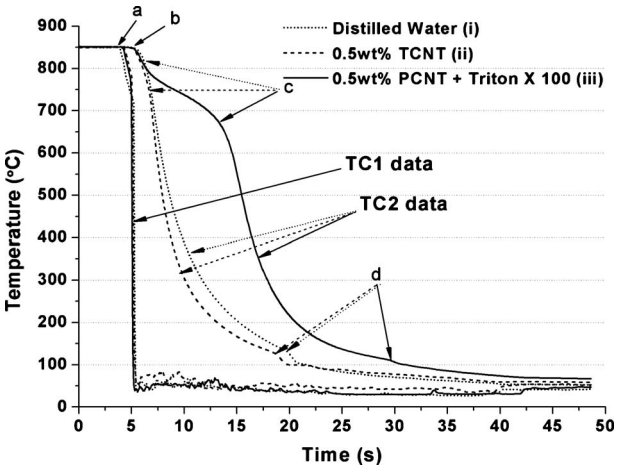

Fig. 7 Measured temperature data during quenching in water and nanofluids

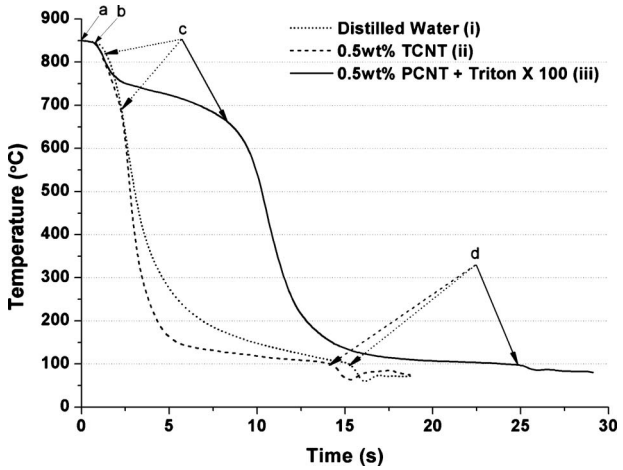

Fig. 8 Computed cooling curve at the probe surface

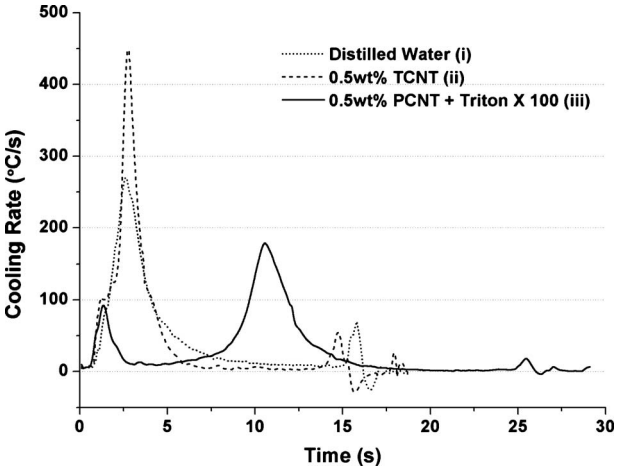

Fig. 9 Cooling rate at the probe surface

made at this stage, as these temperatures were recorded at 2 mm below the probe's surface. There would be a temperature gradient from the surface to the core of the quench probes as the heat transfer inside the material is governed by its thermal diffusivity. Thus, the temperature recorded at TC2 at any instant would be higher and its corresponding cooling rate would be slower than that at the probe's surface.

5.2 Temperature and Cooling Rate at the Quenched Surface. The unknown heat flux and temperature at the quenched surface were computed through the IHC method by using TC2 temperature data (from a of the cooling curves) as input. The computation was carried out until the recorded temperature reached ~90°C. The calculated surface temperature for different cases is plotted in Fig. 8 and it clearly indicates that the drop in the surface temperature in case (ii) is faster than case (i), but it is slower in case (iii) as compared with case (i). Case (iii) is appearing odd because of the prolonged vapor blanket stage. The vapor blanket stage of case (ii) is considerably longer than case (i), but much lesser than case (iii).

The corresponding cooling rates at the surface are calculated for all the cases and plotted in Fig. 9 and it clearly shows the higher peak cooling rate in case (ii) than in case (i), which is due to the presence of CNTs. The peak cooling rate recorded in case (iii) is lower than case (i) and is due to the presence of surfactant in the nanofluid. In case (iii), there is another peak in the cooling rate plot within the film boiling. The film boiling regime of case (iii) has taken place for nearly 8 s, which is significantly longer than the other two cases. Since a considerable portion of the cooling curve is spent in the film boiling, the overall heat transfer is hindered in case (iii).

When the surface temperature reaches ~100°C, there is a sudden drop in the cooling curve (Fig. 8) in all the cases. This represents the onset of convective stage during cooling, and the quenchant completely wets the probe surface (without any bubbles) since boiling of the quenchant (water) ceases at this temperature. However, this drop is not appreciable in case (iii) when compared with the other two cases. A small variation in this temperature can be observed and is due to the fact that the addition of CNTs or surfactant could have altered the boiling point of water slightly. Also, the wetting characteristics of different quenchants vary considerably (Fig. 3); especially, it is significant in case (iii) because of the presence of the surfactant. The peak cooling rate and its time of occurrence are given in Table 1 for all the cases. The increase in the peak cooling rate in case (ii) is 66% when compared with case (i), and the decrease in the peak cooling rate in case (iii) is 33% than in case (i). The reason for the variation in the cooling rates is discussed in the next section with respect to the heat flux.

The overall improvement in the heat transfer during quenching of case (ii) can be attributed to the higher effective thermal conductivity as observed by other researchers. The mechanisms of heat flow in nanofluids have been discussed in detail by Keblinski et al. [18] with respect to (i) the Brownian motion, (ii) the molecular level liquid layering at the liquid/particle interface, (iii) the nature of heat transport (ballistic phonon effects), and (iv) the effect of nanoparticle clustering. Das et al. [19] substantiated the Brownian motion and nanoconvection induced by Brownian motion effects on the heat transfer rate in nanofluids, and Choi [9] also demonstrated some of the above mechanisms as a basis for the improved heat transfer rates in nanofluids. However, Buongiorno et al. [29] observed that experimental confirmation of these mechanisms had been weak and some had been openly questioned. They also observed that the possibility of very large thermal conductivity enhancement in nanofluids was a hotly debated topic.

The higher cooling rate provided by case (ii) is advantageous and comparable to the intensive quenching process [7,8]. The IQ process states that the very high cooling rate at the surface would induce a martensite formation at the core simultaneously as martensite forms at the surface. This would reduce the residual tensile stresses at the surface and in turn reduce the probability of quench crack. The IQ technique has proven this theory by providing higher and uniform cooling rate over the part surface by agitating the quenchant at a faster rate. The benefits of the IQ technique may also be applicable to the parts quenched in the CNT nanofluid prepared without any surfactant. However, the benefits are yet to

Table 1 Peak cooling rate, heat flux, and its time and temperature of occurrence

Case	Quenchant	Peak cooling rate (°C/s)	Time (s)	Peak heat flux (kW/m^2)	Time (s)	Surface temperature (°C)
(i)	Distilled water	270.5	2.6	261.43	3.1	485.2
(ii)	DI water+TCNT	448.8	2.8	359.36	3.0	409.8
(iii)	DI water+PCNT+surfactant	179.2	10.6	196.29	11.1	358.9

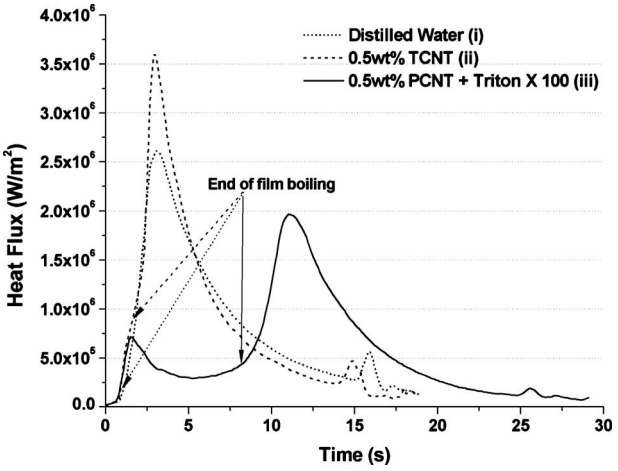

Fig. 10 Transient heat flux at the quenched surface

be quantified. But, a certain additional benefit of using CNT nanofluid having no surfactant over intensive quenching technique is that the former can be used for parts having any intricate shapes. It is one of the limitations of IQ (as reported) that the parts with intricate shapes could not be provided rapid and uniform cooling. It is possible to overcome this limitation with the nanofluids because nanoparticles present in the nanofluids are responsible for faster cooling and can reach any intricate shapes to provide the faster and uniform cooling.

5.3 Heat Flux During Quenching in Different Quenchants. The variation in the surface heat flux is plotted as a function of time in Fig. 10 for different quenchants. The heat flux is also plotted as a function of the surface temperature in Fig. 11 for all the cases, which is referred to as conventional boiling curve during quenching. The heat flux starts from zero, which corresponds with the instant of probe's removal from the furnace and rises slowly to ~ 65 kW/m^2 within 1 s. This increase in the heat flux is caused by the heat transfer due to natural convection and radiation when the probes traveled in air before its full immersion. A slight variation in this initial value of the heat flux for different cases is due to the fact that the probes were transferred manually from the furnace to the quenchant. Then, the heat flux increases rapidly to reach a peak value within a very short period and drops down as the probes tend to attain equilibrium temperature with the quenchant. The boiling curve during quenching has two peaks for cases (i) and (ii): (1) the first peak heat flux within the nucleate boiling stage and (2) the second peak within the convective stage of cooling. Whereas case (iii) has three peaks, the first peak within the film boiling stage and the remaining two are the same as that of the other two cases.

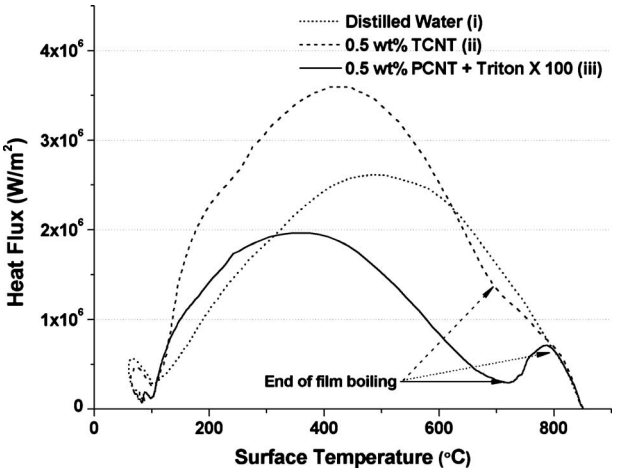

Fig. 11 Boiling curve during quenching in different fluids

5.3.1 Film Boiling in Water and CNT Nanofluids. During film boiling, the heat flux increases rapidly upon full immersion and a film of vapor forms around the probe surface. Once this film of vapor formed, the heat transfer rate is reduced as the film of vapor acts as an insulator to the flowing heat and the slope of the boiling curve slows down. This film of vapor exists as long as the heat transfer across the interface exceeds the amount of heat that is needed to maintain a maximum vapor per unit area [1]. When the heat transfer across the interface is not adequate to maintain this maximum vapor per unit area, the film of vapor breaks down and leads to the next stage of cooling. The length of the film boiling is longer in case (iii) followed by case (ii) and then by case (i). The end of film boiling is marked in Figs. 10 and 11 where the slope of the heat flux curves starts increasing. The film boiling regime is barely distinguishable in case (i) from the next stage of boiling curve and its length is not so significant as compared with cases (ii) and (iii).

Case (ii) has considerably a lengthy vapor phase and the end of this phase is characterized by a small change in the slope at $\sim$2.0 s (Fig. 10) or when the surface temperature reached $\sim$700°C (Fig. 11). The wettability of case (ii) quenchant is higher than that of case (i) quenchant (Fig. 4) and resulted in a lengthy film boiling stage during quenching in case (ii). This is in accordance with the findings of Narayan Prabhu and Fernades [10] during their investigation on water based alumina nanofluids on a stainless steel substrate. Thus, the nanoparticles present in the nanofluid have a significant effect on the film boiling during quenching, which is against the conclusion of Kim et al. [11]. The interference of the CNTs is not sufficient, because of its nanosize, to break the film of vapor, which is against the findings of Chopkar et al. [14] who stated that the presence of nanoparticles possibly helped in breaking down the vapor blanket around the hot body and facilitated efficient heat removal.

Case (iii) has a well distinguishable film boiling stage (Figs. 10 and 11). The film boiling in cases (ii) and (iii) is nearly identical until the formation of the complete film of vapor. Once the complete film of vapor is formed, the heat flux drops down drastically in case (iii) than in case (ii). The surfactant present in case (iii) augmented the vapor formation at the probe surface and the vapor characteristics could be different. This offers a higher resistance to the heat flow, and the heat transfer rate is reduced significantly. Thus, after reaching a peak within the film boiling stage, the heat flux drops down drastically and remains almost flattened until 8 s (Fig. 10) or when the surface temperature reached 720°C (Fig. 11). The surface temperature at which the film boiling ceased in case (iii) is higher than in case (ii). But, on the time scale, the probe surface has taken 8 s to reach 720°C in case (iii), whereas it is only 2 s to reach 700°C in case (ii). This suggests that the size of vapors formed in case (iii) should have been larger and more stable because of the presence of surfactant in the nanofluid.

5.3.2 Nucleate Boiling in Water and CNT Nanofluids. When the film of vapor collapses, it results in small probe-water contact and leads to violent boiling. This is the start of nucleate boiling stage, and the heat transfer rate increases rapidly during this stage. The slope of the boiling curve increases and peaks within a short time in cases (i) and (ii) from the instant of full immersion, but only after 11 s in case (iii) due to the prolonged film boiling stage. The peak heat flux, its time of occurrence, and corresponding surface temperature are given in Table 1 for different cases. The time corresponding to the peak heat flux varies significantly for the nanofluid prepared with surfactant than the other two quenchants, as pointed out earlier. The peak heat flux is higher in case (ii) followed by cases (i) and (iii). With respect to time and surface temperature, this peak has occurred first in case (i) followed

Fig. 12 Quench probes quenched in (*a*) water and (*b*) TCNT nanofluid

by cases (ii) and (iii). The increase in the peak heat flux in case (ii) is 37.5% as compared with case (i) and the decrease in the peak heat flux in case (iii) is 24.9% as compared with case (i). The enhancement in the peak heat flux and peak cooling rate in case (ii) is mainly attributed to the effective higher thermal conductivity of the CNT nanofluid.

There is another possible reason for the improved heat transfer performance of the CNT nanofluid (case ii) apart from the increased thermal conductivity of the CNT nanofluid. The unwashed quench probes after quenching in water and CNT nanofluid (case ii) are shown in Fig. 12. The probe quenched in the CNT nanofluid looks darker in appearance than that quenched in water. This suggests that during quenching, CNT particles get deposited onto the probe surface. The fouling of CNTs onto the probe surface also contributes to the higher heat transfer rates during quenching in the CNT nanofluid apart from the other reasons such as Brownian motion, etc.

The peak heat flux has dropped down in case (iii), the other CNT nanofluid prepared with surfactant. The drop in the peak heat flux and peak cooling rate in case (iii) than in case (i) reveals that the surfactant effect is predominant than the effect of CNTs on quenching heat transfer. The surface temperatures at which the nucleate boiling commenced for cases (ii) and (iii) are 700°C and 720°C, respectively, and do not vary much but the drop in the peak heat flux in case (iii) is almost 60% as compared with case (ii). The presence of surfactant in the nanofluid has increased the viscosity significantly (Fig. 4). The increase in viscosity of nanofluid increases the shear at the liquid-vapor interface and consequently decreases the vapor removal rate according to Lotfi and Shafii [12]. Thus, the bubbles nucleated during the nucleate boiling stage are not leaving fast from the nucleation sites and block the nucleation sites. This reduces the heat transfer rate to a large extent during nucleate boiling. Moreover, the increased viscosity of case (iii) would hinder the Brownian motion of CNTs within the nanofluid. Thus, there is a big difference between the slope of the boiling curves of cases (ii) and (iii). After reaching a peak value, the heat flux decreases throughout the remaining portion of the boiling curve, rapidly at first and then moderately representing that the degree of violent boiling is getting reduced during the nucleate boiling as the surface temperature drops down continuously.

5.3.3 Convective Boiling in Water and CNT Nanofluids. The convective stage of cooling commences once the surface temperature of the probe reaches nearly 100°C for all the cases (Fig. 11) as the boiling comes to an end. The heat transfer rate during the convective stage is only by convection and is lesser. Another peak in the heat flux is occurring during this stage (at the near end of quenching in Figs. 10 and 11) in all the cases and their magnitude is not so significant as compared with the first peak heat flux. The occurrence of this peak could be due to complete wetting of the probe surface without any bubbles [1]. Thus, there is a local increase in the heat flux but lasts only for a shorter period of about 1–2 s. This results in a sudden drop and consequent small rise in the cooling curves when the probe surface temperature reaches ~100°C (Fig. 8). The increase in the heat flux does not commence exactly at the same temperature for all the cases, especially case (iii), and this minor difference is due to the presence of CNTs and surfactant, which should have altered the boiling point of the water as discussed already.

The effect of CNT concentration and agitation rate on the surface heat flux during quenching in CNT nanofluids has been studied by Babu and Prasanna Kumar [25]. The peak heat flux increased with an increase in CNT concentration up to 0.5 wt % and then started decreasing with further increase in CNT concentration.

6 Summary and Conclusions

This experimental work demonstrated the use of nanofluids to improve the quenching heat transfer. Water based CNT nanofluids were prepared and successfully used for a practical quenching application. The temperature and heat flux at the quenched surface were calculated through an IHC method. The effect of CNT nanofluid on the quenching heat transfer was analyzed based on the estimated heat flux and surface temperature at the quenched surface. Also, the use of surfactant in the preparation of CNT nanofluid was studied during quenching of SS probes in CNT nanofluid without agitation. The conclusions drawn from this experimental work are summarized as follows.

1. There were two peaks in the surface heat flux: (i) the first peak heat flux during the nucleate boiling and (ii) the second peak heat flux when the probe surface reached ~100°C for water and CNT nanofluid without any surfactant. But, in the case of CNT nanofluid prepared with surfactant, there were three peaks; the first peak within the film boiling stage and the remaining two were similar as in the other cases.
2. The use of nanofluids as quenchant improved the quenching heat transfer rate significantly, but the method of preparation played a major role in determining the heat transfer performance of the nanofluids for quenching application.
3. Nanofluids prepared without surfactant enhanced the quenching heat transfer, and the peak surface heat flux was improved by 37.5% as compared with that of water.
4. The overall increase in the heat transfer rates during quenching in CNT nanofluids prepared without any surfactant was due to the higher effective thermal conductivity of CNT nanofluids and also due to fouling of CNTs onto the probe surface.
5. Nanofluid prepared with surfactants hindered the heat transfer during quenching, and the peak heat flux during nucleate boiling was reduced by 24.9% due to the lengthy film boiling as compared with water.
6. Nanofluids for quenching application should strictly avoid any use of surfactants while preparing the nanofluids if the intention is to improve the heat transfer rate.
7. CNT nanofluid prepared without surfactant had a slightly lengthy film boiling as compared with water and if it can be suppressed by agitation or other means, still higher heat transfer rates can be achieved and may evolve as an alternate quench technique to intensive quenching.
8. Though the benefits of the IQ process are applicable to quenching in CNT nanofluids, the exact consequences of higher cooling rate achieved by nanofluids are to be thoroughly investigated.

References

[1] Babu, K., and Prasanna Kumar, T. S., 2010, "Mathematical Modeling of Surface Heat Flux During Quenching," Metall. Mater. Trans. B, **41**(1), pp. 214–224.

[2] Beck, J. V., Blackwell, B., and St. Clair, C. R., Jr., 1985, *Inverse Heat Conduction: Ill-Posed Problems*, Wiley, New York.

[3] Prasanna Kumar, T. S., 2004, "A Serial Solution for the 2-D Inverse Heat Conduction Problem for Estimating Multiple Heat Flux Components," Numer. Heat Transfer, Part B, **45**, pp. 541–563.

[4] Prasanna Kumar, T. S., and Kamath, H. C., 2004, "Estimation of Multiple Heat Flux Components at the Metal/Mold Interface in Bar and Plate Aluminum Alloy Castings," Metall. Mater. Trans. B, **35**, pp. 575–585.

[5] Arunkumar, S., Sreenivas Rao, K. V., and Prasanna Kumar, T. S., 2008, "Spatial Variation of Heat Flux at the Metal-Mold Interface Due to Mold Filling Effects in Gravity Die-Casting," Int. J. Heat Mass Transfer, **51**, pp. 2676–2685.

[6] Sarmiento, G. S., Chen, X., Vega, J., Totten, G., Raynoldson, R., Huynh, L., and Meekisho, L., 2000, "A Comparison of Cooling Curve Analysis Using Inc-Phatran and Winprobe," *Proceedings of the 20th Heat Treating Conference*, K. Funatani and G. E. Totten, eds., St. Louis, MO, Vols. 1&2, pp. 659–665.

[7] Aronov, M. A., Kobasko, N. I., and Powell, J. A., 1999, "Practical Application of the Intensive Technology Process for Steel Parts," Ind. Heat., April, pp. 59–63.

[8] Freborg, A. M., Lynn Ferguson, B., Aronov, M. A., Kobasko, N. I., and Powell, J. A., 2003, "Intensive Quenching Theory and Application for Imparting High Residual Surface Compressive Stresses in Pressure Vessel Components," ASME J. Pressure Vessel Technol., **125**, pp. 188–194.

[9] Choi, S. U. S., 2009, "Nanofluids: From Vision to Reality Through Research," ASME J. Heat Transfer, **131**(3), p. 033106.

[10] Narayan Prabhu, K., and Fernades, P., 2008, "Nanoquenchants for Industrial Heat Treatment," J. Mater. Eng. Perform., **17**, pp. 101–103.

[11] Kim, H., DeWitt, G., McKrell, T., Buongiorno, J., and Hu, L., 2009, "On the Quenching of Steel and Zircaloy Spheres in Water-Based Nanofluids With Alumina, Silica and Diamond Nanoparticles," Int. J. Multiphase Flow, **35**, pp. 427–438.

[12] Lotfi, H., and Shafii, M. B., 2009, "Boiling Heat Transfer on a High Temperature Silver Sphere in Nanofluid," Int. J. Therm. Sci., **48**, pp. 2215–2220.

[13] Chopkar, M., Das, P. K., and Manna, I., 2006, "Synthesis and Characterization of Nanofluid for Advanced Heat Transfer Applications," Scr. Mater., **55**, pp. 549–552.

[14] Chopkar, M., Kumar, S., Bhandari, D. R., Das, P. K., and Manna, I., 2007, "Development and Characterization of Al_2Cu and Ag_2Al Nanoparticle Dispersed Water and Ethylene Glycol Based Nanofluid," Mater. Sci. Eng., B, **139**, pp. 141–148.

[15] Park, K., and Jung, D., 2007, "Enhancement of Nucleate Boiling Heat Transfer Using Carbon Nanotubes," Int. J. Heat Mass Transfer, **50**, pp. 4499–4502.

[16] Ding, Y., Alias, H., Wen, D., and Williams, R. A., 2006, "Heat Transfer of Aqueous Suspensions of Carbon Nanotubes (CNT Nanofluids)," Int. J. Heat Mass Transfer, **49**, pp. 240–250.

[17] Xie, H., Lee, H., Youn, W., and Choi, M., 2003, "Nanofluids Containing Multiwalled Carbon Nanotubes and Their Enhanced Thermal Conductivities," J. Appl. Phys., **94**, pp. 4967–4971.

[18] Keblinski, P., Phillpot, S. R., Choi, S. U. S., and Eastman, J. A., 2002, "Mechanisms of Heat Flow in Suspensions of Nano-Sized Particles (Nanofluids)," Int. J. Heat Mass Transfer, **45**, pp. 855–863.

[19] Das, S. K., Putra, N., Thiesen, P., and Roetzel, W., 2003, "Temperature Dependence of Thermal Conductivity Enhancement for Nanofluids," ASME J. Heat Transfer, **125**, pp. 567–574.

[20] Chopkar, M., Sudarshan, S., Das, P. K., and Manna, I., 2008, "Effect of Particle Size on Thermal Conductivity of Nanofluid," Metall. Mater. Trans. A, **39**(7), pp. 1535–1542.

[21] Liu, M., Lin, M., Huang, I., and Wang, C., 2005, "Enhancement of Thermal Conductivity With Carbon Nanotube for Nanofluids," Int. Commun. Heat Mass Transfer, **32**, pp. 1202–1210.

[22] Amrollahi, A., Hamidi, A. A., and Rashidi, A. M., 2008, "The Effects of Temperature, Volume Fraction and Vibration Time on the Thermo-Physical Properties of a Carbon Nanotube Suspension (Carbon Nanofluid)," Nanotechnology, **19**, p. 315701.

[23] Chen, L., Xie, H., Li, Y., and Yu, W., 2008, "Nanofluids Containing Carbon Nanotubes Treated by Mechanochemical Reaction," Thermochim. Acta, **477**, pp. 21–24.

[24] Joshi, R., Engstler, J., Nair, P. K., Haridoss, P., and Schneider, J. J., 2008, "High Yield Formation of Carbon Nanotubes Using a Rotating Cathode in Open Air," Diamond Relat. Mater., **17**, pp. 913–919.

[25] Babu, K., and Prasanna Kumar, T. S., 2011, "Effect of CNT Concentration and Agitation on Surface Heat Flux During Quenching in CNT Nanofluids," Int. J. Heat Mass Transfer, **54**, pp. 106–117.

[26] Lee, J., Kim, M., Hong, C. K., and Shim, S. E., 2007, "Measurement of the Dispersion Stability of Pristine and Surface-Modified Multiwalled Carbon Nanotubes in Various Nonpolar and Polar Solvents," Meas. Sci. Technol., **18**, pp. 3707–3712.

[27] Rastogi, R., Kaushal, R., Tripathi, S. K., Sharma, A. L., Kaur, I., and Bharadwaj, L. M., 2008, "Comparative Study of Carbon Nanotube Dispersion Using Surfactants," J. Colloid Interface Sci., **328**, pp. 421–428.

[28] Chen, X., Meekisho, L., and Totten, G. E., 1999, "Cooling Curve Analysis Using $1\times2''$ Stainless Steel Probe," *Proceedings of the 19th Heat Treating Conference*, S. J. Midea and G. D. Pfaffmann, eds., Cincinnati, OH, pp. 453–460.

[29] Buongiorno, J., Venerus, D. C., Prabhat, N., McKrell, T., Townsend, J., Christianson, R., Tolmachev, Y. V., Keblinski, P., Hu, L., Alvarado, J. L., Bang, I. C., Bishnoi, S. W., Bonetti, M., Botz, F., Cecere, A., Chang, Y., Chen, G., Chen, H., Chung, S. J., Chyu, M. K., Das, S. K., Di Paola, R., Ding, Y., Dubois, F., Dzido, G., Eapen, J., Escher, W., Funfschilling, D., Galand, Q., Gao, J., Gharagozloo, P. E., Goodson, K. E., Gutierrez, J. G., Hong, H., Horton, M., Hwang, K. S., Iorio, C. S., Jang, S. P., Jarzebski, A. B., Jiang, Y., Jin, L., Kabelac, S., Kamath, A., Kedzierski, M. A., Kieng, L. G., Kim, C., Kim, J., Kim, S., Lee, S. H., Leong, K. C., Manna, I., Michel, B., Ni, R., Patel, H. E., Philip, J., Poulikakos, D., Reynaud, C., Savino, R., Singh, P. K., Song, P., Sundararajan, T., Timofeeva, E., Tritcak, T., Turanov, A. N., Vaerenbergh, S. V., Wen, D., Witharana, S., Yang, C., Yeh, W.-H., Zhao, X.-Z., and Zhou, S.-Q., 2009, "A Benchmark Study on the Thermal Conductivity of Nanofluids," J. Appl. Phys., **106**, p. 094312.